DOI: 10.1051/epjconf/202328305003

Searches for Lorentz Invariance Violation at the Pierre Auger Observatory

Caterina Trimarelli[1,2,*] for the Pierre Auger Collaboration[3,**]

[1]Università dell'Aquila
[2]INFN Laboratori Nazionali del Gran Sasso, Assergi (L'Aquila), Italy
[3]Observatorio Pierre Auger, Av. San Martín Norte 304, 5613 Malargüe, Argentina

Abstract. Lorentz Invariance (LI) requires the space-time structure to be the same for all observers, but various quantum gravity theories suggest that it may be violated when approaching the Planck scale. Even a small violation of LI could easily affect the Ultra-High-Energy Cosmic Ray (UHECRs) propagation on a cosmological scale. Moreover, at the extreme energies, like those available in the collisions of UHECRs in the atmosphere, one should also expect a change in the development of Extensive Air-Showers (EAS). In this contribution, Lorentz Invariance Violation (LIV) has been introduced as a perturbation term in the single particle dispersion relation considering a phenomenological approach. As a result, the kinematics of the interactions in both the extragalactic propagation and in the shower development in the atmosphere is affected. The comparison between the model predictions and the data measured by the Pierre Auger Observatory are considered to constrain the LIV scenarios. The impact of LIV has been tested considering the measured energy spectrum and the composition and the resulting upper limits on the photon flux. Finally, the effects on the shower cascade in the atmosphere are studied considering the muon content distribution.

1 Introduction

Violations of Lorentz symmetry could change the energy threshold of photo-hadronic interactions; in particular, depending on the composition of the UHECRs at the highest energies, the attenuation length of photo-meson production or photo-disintegration may become extremely large and suppress particle interaction during propagation in the extragalactic space [1–4]. As a consequence, the existing evidence of the suppression of the flux at the highest energies [5] can be used to put a limit on LIV. However, data from the Pierre Auger Observatory can be interpreted in a scenario in which the origin of the suppression is due to the maximum acceleration energy at the sources rather than to interactions with the background radiation. In this scenario, UHECR data can no longer yield bounds on LIV. On the other hand, violation of Lorentz invariance can be tested by deriving limits on violation parameters from UHECR phenomena other than propagation. In particular, LIV can be tested by searching the best description of the UHECR observables, under LIV assumptions, as already done in [6–9]. Moreover, to set limits in the electromagnetic sector the upper limits on the UHE photon flux found by the Pierre Auger Observatory is compared with the result produced in the presence of LIV.

An alternative approach to constrain LIV models is that, depending on the strength of the violation, the high energy available in the collision of cosmic rays with the atmosphere can lead to modifications of the shower development with respect to the standard LI case [10].

2 The Pierre Auger Observatory and datasets

The Pierre Auger Observatory [11], located on a vast plain in Argentina, just northeast of the town of Malargüe, in the Province of Mendoza, 1440 m above the sea level, is the largest observatory to detect UHECRs ever built and it has been in operation since 2004. It covers an area of 3000 km^2 with a Surface Detector array (SD) overlooked by a Fluorescence Detector (FD). The SD consists of 1660 water-Cherenkov detectors arranged in a triangular grid operating with a nearly 100% duty cycle. Each SD station detects at ground level the secondary particles of the EAS produced by the primary UHECR interacting in the atmosphere. The FD consists of a set of telescopes that measure the UV fluorescence light from nitrogen molecules excited by the EAS particles along their path in the atmosphere. FD operations are limited to clear moonless nights, resulting in a duty cycle of about 15%. This hybrid detection technique combines the calorimetric measurement of the shower energy through fluorescent light with the high-statistics data of the surface array. The combination of the information from both techniques results in a quasi-calorimetric determination of the energy scale, a geometric direction reconstruction and an estimator of the primary particle mass.

In this paper, I summarize some recent results about the searches of Lorentz Invariance Violation using the data

*e-mail: caterina.trimarelli@aquila.infn.it
**e-mail: spokespersons@auger.org
Full author list: https://www.auger.org/archive/authors_2022_10.html

measured by the Pierre Auger Observatory described in [9, 10].

3 Lorentz Invariance Violation framework

A well established phenomenological approach to introduce LIV effects consists of adding effective terms in the dispersion relation of particles [12]. The resultant dispersion relation can be expressed as:

$$E_i^2 - p_i^2 = m_i^2 + \epsilon_i s_i^2, \tag{1}$$

where i defines the particle, E, m and p correspond, respectively, to the energy, mass and momentum of the particle, and s can be chosen to be either the energy or the momentum (for ultra-relativistic particles). In the following we consider $s = p$. At $p \ll M_{\rm Pl}$, the factor ϵ can be expanded as a polynomial series as a function of p, so that:

$$E_i^2 - p_i^2 = m_i^2 + \sum_{n=0}^{N} \delta_i^{(n)} p_i^{2+n}, \tag{2}$$

where n is the LIV order. The parameters $\delta_i^{(n)}$ are independent for each particle species and define the energy scale associated with the violation. It can be noticed that the LIV parameters is sometimes introduced as:

$$\delta_i^{(n)} = \frac{\eta_i^{(n)}}{M_{\rm Pl}^n} \tag{3}$$

where $M_{\rm Pl} \approx 1.22 \cdot 10^{22}$ GeV/c^2 is the Planck mass. If we assume that only the lowest-order non-vanishing term has a non-negligible effect it is possible to set individual limits on $\delta_i^{(n)}$.

Considering Eq. 3, the modified dispersion relation (for only the leading term) can be expressed in terms of the dimensionless constant parameter $\eta_i^{(n)}$ as follows:

$$E_i^2 - p_i^2 = m_i^2 + \eta_i^{(n)} \frac{p_i^{n+2}}{M_{\rm Pl}^n} \tag{4}$$

4 LIV searches in the extragalactic propagation of UHECRs

In this section, the searches for LIV signatures reported in [9] in the cosmic-ray interactions during their propagation through the universe are described. In that work, we consider the modified dispersion relation in terms of $\delta_i^{(n)}$ (see Eq. 2). In particular, new bounds for the LIV parameter $\delta_i^{(n)}$ are found using the data collected by the Pierre Auger Observatory. The kinematics and the energy thresholds of interactions are modified once the LIV terms become comparable to the squared masses involved. Two independent LIV sectors are tested. Limits on the electromagnetic sector are set considering that, at sufficiently high energies, the cosmogenic photons produced by cosmic ray interactions with the background radiation fields could be subluminal and be attenuated much less than in the LI case over cosmological distances. On the other hand, for the hadronic sector, how the modifications on the cosmic rays interactions affect the energy spectrum and the mass composition at Earth is considered.

Signatures of LIV are studied considering a specified UHECR scenarios. We consider isotropically distributed sources with $(1-z)^m$ cosmological evolution emitting an energy spectrum given by:

$$\frac{dN_A}{dE} = J_0 f_A \left(\frac{E}{10^{18}\text{eV}}\right)^{-\Gamma} \times \begin{cases} 1, & R < R_{\rm cut} \\ \exp(1 - R/R_{\rm cut}), & R \geq R_{\rm cut} \end{cases} \tag{5}$$

where z is the redshift, Γ is the spectral index at the injection, $R_{\rm cut}$ is the cutoff rigidity, f_A is the fraction of nuclei with mass A, and J_0 is the normalization factor of the flux. UHECRs interact with photon backgrounds and at these energies, the most important photon backgrounds are the cosmic microwave background (CMB) and the extra-galactic background light (EBL). Given the uncertainties in the models, two EBL distributions and two photo-nuclear cross section models among the UHECR propagation models are used in this study [13]. To compare the events at Earth with the $X_{\rm max}$ data, the mass composition is transformed into an $X_{\rm max}$ distribution with the use of EAS simulations according to different hadronic interaction models. The $X_{\rm max}$ distributions are parameterized using the Gumbel functions [14]. Finally, a UHECR scenario is here defined by the set of parameters from the source, the propagation model and the hadronic interaction model.

4.1 LIV limits on the electromagnetic sector

In this section, the LIV signatures in the electromagnetic sector are briefly described. The interaction of UHECRs with the background radiation produces pions as studied by Greisen [15], Zatepin and Kuzmin (GZK) [16]. The neutral pions decay into UHE photons, hereinafter call GZK photons, and are absorbed during propagation due to electron-positron pair production with background photon fields [17]. In presence of LIV in the photon sector, the kinematics of this pair production is changed. Considering Eq. 2 for subluminal LIV ($\delta_\gamma < 0$), the modified mean free path can be retrieved. Figure 1 shows the ratio between the LIV and LI mean free paths for different LIV parameters corresponding to the LIV order $n = 0$. The main effect consists on a significant increase of the mean free path above a critical energy. The same result is found for LIV at first and second orders. As a consequence, for negative values of the LIV parameters, fewer UHE photons will be absorbed and, the arriving flux of these particles will be larger. To quantify the LIV effects, the pair production of UHE photons is simulated in the extragalactic space under LIV hypotheses and the UHE photon flux are used to test LIV in the electromagnetic sector. In particular, the LIV-modified mean free path is implemented in the software packages CR-Propa3/EleCa [18, 19] in order to obtain the arriving GZK photon flux. Further simulation details can be found in [9]. Comparing the resulting photon flux in presence of LIV with the upper limits imposed by the Pierre Auger Observatory a new bound for

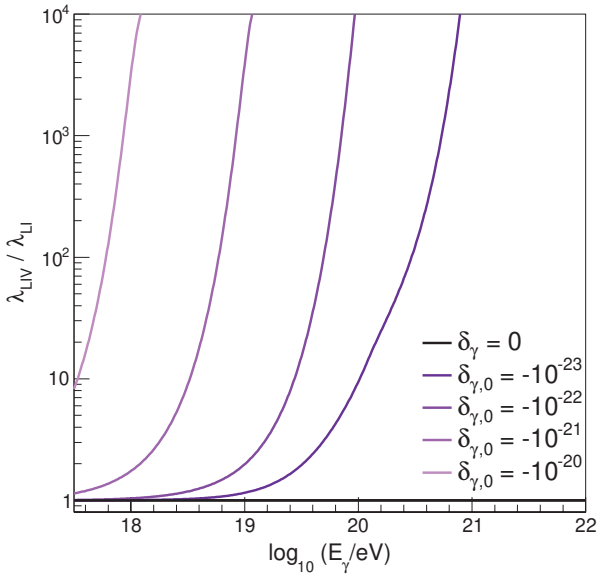

Figure 1. Ratio of the mean free path of pair production as a function of energy when LIV and LI are considered. The black line represents the LI case, while the shades of purple represent different LIV coefficients. Figure from [9].

the LIV parameters for different LIV orders is found. Different UHECR scenarios are taken into account. In Figures 2, the results are shown for photons produced in extragalctic propagation by UHECRs with an additional proton component at high energies. The Gilmore EBL model [20], Talys [21] cross-section and the EPOS LHC interaction model [22] are used. In particular, the Figures show the simulated GZK photon flux arriving at Earth under this scenario for LIV orders $n = 1, 2$ compared to the measured upper limits on the photon flux from the Pierre Auger Observatory. For some coefficients, the simulated LIV GZK photon flux is higher than the upper limits. The direct comparison of the simulation to the data give new limits for the LIV parameters: $\delta_\gamma^{(1)} > -10^{-40}$ eV^{-1}, $\delta_\gamma^{(2)} > -10^{-58}$ eV^{-2}.

4.2 LIV limits on the hadronic sector

In this section, the LIV signatures in the hadronic sector are described. During the propagation, the UHECRs interact with the background radiation and the kinematics of the dominant energy losses, photo-pion production and photodisintegration are modified under LIV assumptions. Only positive values of the LIV parameter $\delta_{\rm had}^{(n)}$ are taken into account. In the superluminal case, above a critical energy the photopion production for protons and the photodisintegration for nuclei change. The number of interactions is reduced and, consequently, the cosmic rays can travel farther than they would do under the LI hypotheses. To quantify the LIV effects both the modified attenuation length for pion production and the LIV modified energy threshold for photodisintegration were implemented in SimProp v2r4 [23]. Simulation details can be found in [9]. In this case instead of considering a fixed scenario, the source parameters and the LIV coefficients are fitted to the energy spectrum and composition from the Pierre Auger Observatory. Spectrum and composition are given by the LIV modified 10^5 events produced with SimProp v2r4 (simulations performed for 5 nuclei). The simulated energy spectrum and composition arriving at Earth are used to fit to the data of the Pierre Auger Observatory for energies above $10^{18.7}$ eV. The fit procedure follows the explanation in [24]. Within each UHECR scenario, the free parameters of the fit are: a) the nuclei fractions, f_A, b) the index of the energy spectrum, Γ, c) the maximum rigidity, $R_{\rm cut}$, d) the normalization factor of the flux, J_0 and e) the LIV coefficient, $\delta_{\rm had}^{(0)}$. The cosmological evolution of the sources was fixed to $m = 0$. For each value of $\delta_{\rm had}^{(0)}$ ranging from 10^{-24} to 10^{-18} in $\log_{10}$ steps of 1 and for the LI case ($\delta_{\rm had}^{(0)}$) a log-likelihood fit was done searching for the combination of the parameters which best describes the data. Comparing the deviances obtained in LIV and LI scenarios limits on $\delta_{\rm had}^{(0)}$ have been imposed. In Figure 3 the energy spectrum and the first two moments of the $X_{\rm max}$ distributions in comparison with these corresponding to the LI case are shown. The comparison between the two panels with LI (left panel) and LIV (right panel) shows the correlation between mass composition and LIV in the fit. Lorentz violation suppresses the interactions during propagation which is compensated with a lighter composition at the sources in order to obtain the same composition on Earth.

5 LIV searches in the air-shower development

In this section, the approach considered to understand and determine the modification that the air-shower development undergoes in presence of LIV is described.

Interpreting the right-hand side of Eq. 4 as an energy dependent mass, $m_{\rm LIV}^2 = m^2 + \eta^{(n)} p^{n+2}/M_{\rm Pl}^n$, the Lorentz factor for a LI violating particle at energy E can be defined as:

$$\gamma_{\rm LIV} = E/m_{\rm LIV} \tag{6}$$

Depending on the value assumed by $\eta^{(n)}$, the LIV effects can be easly analyzed considering the lifetime of the considered particle $\tau = \gamma_{\rm LIV}\tau_0$, where τ_0 is the lifetime at rest, that will change accordingly. For negative/positive values of $\eta^{(n)}$ the lifetime of the particle should increase/decrease with respect to the LI case producing modifications in the EAS development which depends both on the energy and the strength of the violation. To understand the expectations, the π^0 decay can be taken into account. The π^0 lifetime as a function of the energy for the standard case and for different values of the LIV parameters is shown in Fig. 4. The energy at which the lifetime evolution deviates from the standard LI case depends both on the order and the strength of the violation. To have a qualitative idea of what one should expect, let us consider the simple model [25] where a primary hadron interacting in the atmosphere produces 2/3 of charged pions $\pi^\pm$ and 1/3 of $\pi^0 s$. In the standard case, charged pions decay producing muons and neutrinos while the neutral ones quickly decay

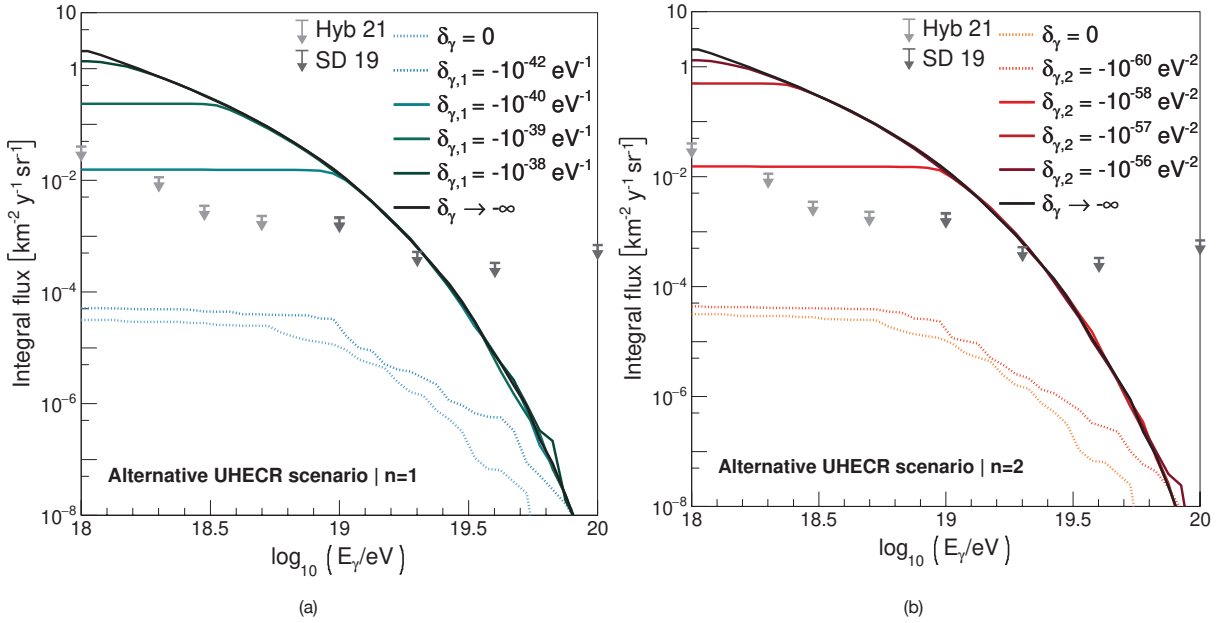

Figure 2. Simulated integral flux of GZK photons as a function of the energy for an alternative scenario with subdominant proton component. Continuous lines show the rejected LIV scenarios. The arrows show the flux determined by analysis of the Pierre Auger Observatory data. LIV at first order (a) and LIV at second order (b). Figures from [9].

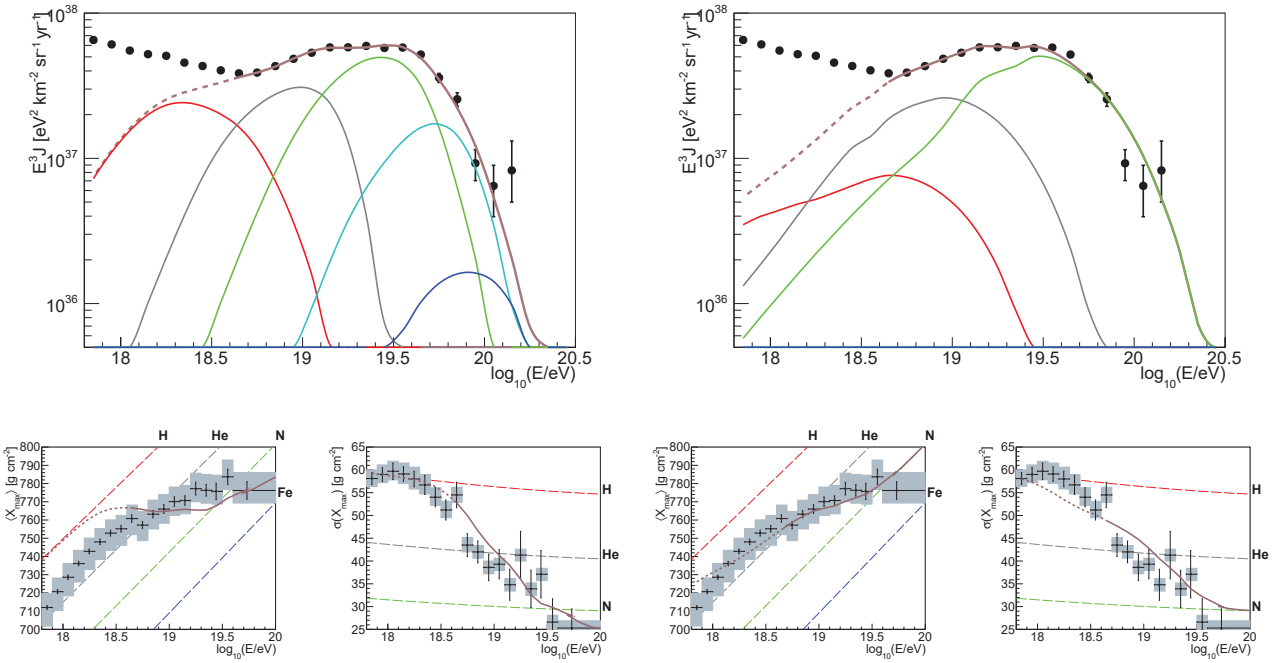

Figure 3. Energy spectrum (top) and first two moments of the $X_{\rm max}$ distributions (bottom), for the LI (left panels) and LIV $\delta^{(0)}_{\rm had} = 10^{-20}$ cases (right panels) for the STGE propagation model compared to the Pierre Auger Observatory data. Partial distributions are grouped according to the mass number as follows: $A = 1$ (red), $2 \le A \le 4$ (grey), $5 \le A \le 22$ (green), $23 \le A \le 38$ (cyan), $39 \le A \le 56$ (blue), total (brown). Dashed brown lines show the energy region not used for the fit. Dashed lines in the bottom panes show simulations predictions for each element. Figures from [9].

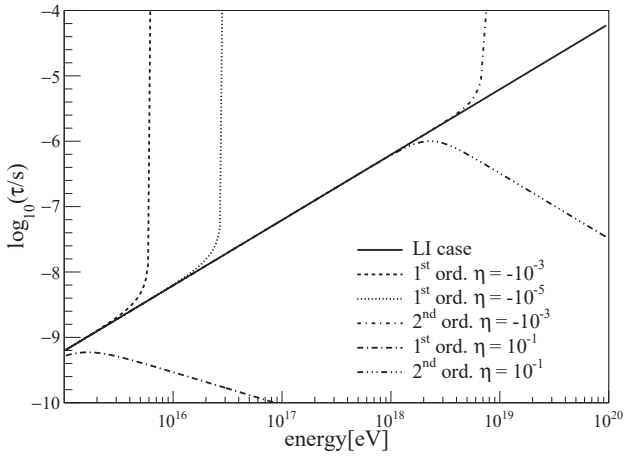

Figure 4. Neutral pion mean lifetime as a function of energy for the Lorentz invariant case and for different strengths of LIV. Figure from [10].

in two photons producing an electromagnetic sub-shower. Otherwise, in the presence of LIV and for negative values of $\eta^{(n)}$, the π^0 lifetime grows and the probability to interact before decaying increases. The re-interacting π^0s will behave as the source of a hadronic sub-showers like those initiated by charged pions. As the energy decreases in the further shower generations, π^0s will start again to produce a standard electromagnetic sub-shower. The consequence is a modification of the shower development in the atmosphere. The amount of energy deposited in the atmosphere will be reduced (i.e. invisible energy going to neutrinos will grow) leading to an underestimation of the primary energy if the event is treated as a standard physics one. Moreover, the position of the shower maximum ($X_{\max}$) [26] will be slightly modified with respect to the standard LI case. In addition, as the muon content correlates with the energy of the hadronic component of the shower, we can expect that the number of muons produced in the EAS will increase and the physical fluctuations will decrease, as almost all the energy is kept into the hadronic component after the first stages of the shower developement, with little room for stochastic leakage to the electromagnetic component [27]. In this work only the effects due to negative values of the η parameter are considered. Our purpose is to find only the lower limit of the bound for LIV at first order.

To quantify the effect of LIV on the shower development, we have performed a library of simulated showers by using CONEX software [28, 29] in both LI and LIV cases. For the violated scenario, the software has been modified by changing the lifetimes of all the unstable particles according to Eq. 6. In particular, in the velocity definition $\beta = \frac{|\mathbf{P}|}{m\gamma}$, the Lorentz factor γ has been replaced with the LIV expression $\gamma_{\rm LIV} = E/m_{\rm LIV}$. The values of $\eta^{(n)}$ considered[1] for this study are -10^{-1}, -10^{-2}, -10^{-3}, -10^{-4}, -10^{-5}, -10^{-6}, -10^{-7}, -10^{-8} and order of the violation $n = 1, 2$. For each value of η, 5000 primary cosmic ray particles have been produced in the energy range between 10^{16} eV and 10^{21} eV, using EPOS LHC [22] and QGSJETII-04 [30] hadronic interaction models and for different primary particle types i.e. proton, helium, nitrogen, silicon and iron.

5.1 The muon content distribution

As a result of the modified air shower simulation in the presence of LIV at first order, we have considered the mean longitudinal profile dE/dx. For larger values of $|\eta|$ (only negative LIV parameters are taken into account) the effects due to the violation increase. In fact, we have found a shift of $X_{\max}$, and a reduction in the height of the maximum energy deposit in the atmosphere.

First of all, the displacement in the position of the maximum of the longitudinal profile leads to different values of $X_{\max}$. The change in the energy threshold of particle decays (mainly neutral pions), consuming the electromagnetic part of the shower faster, generates the effect to move the shower maximum to higher altitudes. This is due to the fact that a proton from the point of view of the shower development is behaving like a heavier nucleus. In fact, in the presence of LIV, the measured mass composition corresponds to a greater fraction of protons at the highest energies. This result has been already used in order to constrain LIV models in a previous work [31] and it is not considered in this contribution.

On the other hand, the reduction in the normalization of the longitudinal profile is linked to a change in the number of muons at the ground. In particular, the calorimetric energy deposited in the atmosphere in the presence of LIV is lower than the standard one. The modification of the energy-momentum relation allows hadronic interactions of neutral pions that contribute to the growth of the hadronic cascade producing an increase in the number of muons, as shown in Fig. 5, where the average number of muons at ground as a function of the primary energy in LI and LIV cases are shown. For proton-induced air showers, the number of muons is considerably increased, in any of the LIV cases considered here, while for iron primaries the effect is in general milder.

These two main effects, caused by the LIV framework, affect the fluctuations of the number of muons. In fact, the ratio of the fluctuations to the average number of muons (hereinafter referred to as relative fluctuations), dominated mostly by the first interaction [27], considerably decreases in the presence of LIV, as shown in Fig. 5, where the relative fluctuations of the number of muons as a function of the primary energy are reported.

Limits on LIV parameter η can be derived comparing the observed strong decrease of the relative fluctuations with the muon fluctuation measurement [32] from the Pierre Auger Observatory. Considering the dependence of the decrease of the relative fluctuations on the different LIV strengths, a new bound for the LIV parameter

[1] Positive values of LIV parameter have been also considered but no effect on the shower development has been found because in these cases, the lifetime of neutral pions, already negligible in the LI case, decreases above the critical energy and the pions decay faster than in the standard one.

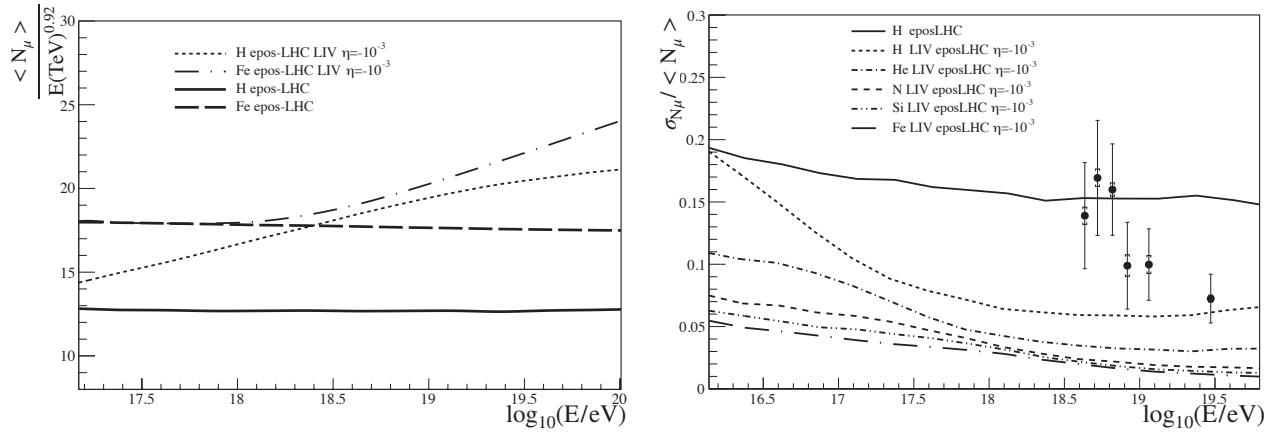

(a) (b)

Figure 5. (a) Average number of muons at ground vs primary energy in LI and LIV cases; (b) Data (black points with error bars) compared to LI and LIV models for the relative fluctuation of the number of muons vs primary energy. The LIV case corresponds to $\eta = -10^{-3}$. The statistical uncertainty is indicated by the error bars. The total systematic uncertainty is indicated by the square brackets. Figures from [10].

$\eta^{(1)}$ has been obtained. To find this, the most conservative LIV model with respect to data, depending on the particular mixture of primary particles, should be considered. In particular, the effects of different composition scenarios on both fluctuations and average number of muons have been taken into account. It can be noticed, referring to Fig. 3 in [32], that the mixture of the two components, p and Fe, gives the maximum value of relative fluctuations. Therefore, the most conservative LIV model corresponds to the ratio of the fluctuations to the average number of muons for a mixture of proton and iron.

We have defined the average number of muons $\langle N_\mu \rangle_{\rm mix}$ and the fluctuations $\mathrm{RMSD}(N_\mu)_{\rm mix}$ for a mixture of p and Fe using the following expressions:

$$\begin{aligned} \langle N_\mu \rangle_{\rm mix}(\alpha;\eta) &= (1-\alpha)\langle N_\mu \rangle_p + \alpha \langle N_\mu \rangle_{Fe} \\ \mathrm{RMSD}^2(N_\mu)_{\rm mix}(\alpha;\eta) &= (1-\alpha)\,\mathrm{RMSD}^2(N_\mu)_p + \\ &\alpha\,\mathrm{RMSD}^2(N_\mu)_{Fe} + \alpha(1-\alpha)(\langle N_\mu \rangle_p - \langle N_\mu \rangle_{Fe})^2 \end{aligned} \quad (7)$$

where α, which depends on the energy, is the relative abundance of iron nuclei and the subscripts p and Fe label the averages and RMSD of pure proton and iron primaries respectively that are retrieved from the air shower simulations. [2] These values have been used to parametrize $\langle N_\mu \rangle$ and the RMSD between $\log_{10}(E/\mathrm{eV}) = 16.5$ and $\log_{10}(E/\mathrm{eV}) = 20$, for $-10^{-3} < \eta < -10^{-15}$ and for different masses. For each value of η, the parameterizations can be used to calculate the expected relative fluctuations for a certain mixture of proton and iron nuclei (hereinafter referred to as mixed relative fluctuations) as:

$$\frac{\sigma_\mu}{\langle N_\mu \rangle}(\alpha;\eta) = \frac{\sqrt{\mathrm{RMSD}^2(N_\mu)_{\rm mix}(\alpha;\eta)}}{\langle N_\mu \rangle_{\rm mix}(\alpha;\eta)} \quad (8)$$

To determine the most conservative LIV model the result of the mixed relative fluctuations for different mixtures of proton-iron composition are considered as a function of the energy. In particular, it has been found that the maximum with respect to α is above all the mixed relative fluctuations for a scan of the relative abundance α between 0 and 1. This effect has been observed for all the violation strengths. Therefore, only if all the curves are below the data points, the maximum with respect to $\alpha(E)$ of Eq. 8 in each energy bin corresponds to the most conservative LIV model. For any LIV parameter value, the most conservative LIV relative fluctuations as a function of the energy can be found without repeating any shower simulation. In Fig. 6, the coloured thin curves represent the maxima with respect to α for the relative fluctuations obtained from the parameterizations considering the η parameter in the range $[-10^{-3}, -10^{-15}]$. Considering only the curves that are below the data, the χ^2 can be calculated as a function of η using each resulting mixed fluctuation and all the experimental data points. In this way, a continuous confidence level to exclude the LIV model has been found. This continuous result allows to determine the strictest lower η parameter bound. As a consequence, the new bound for $\eta^{(1)}$ is $[-5.95 \cdot 10^{-6}, 10^{-1}]$ at 90.5% of CL.

In conclusion, we have found a new lower bound of the η parameter range of values using the maximum relative fluctuation for a mixed initial proton-iron composition for LIV at first order. A similar approach using the minimum of the relative fluctuation with respect to α could lead to the definition of a negative upper bound of the LIV parameter.

[2] $\langle N_\mu \rangle_p$, $\langle N_\mu \rangle_{Fe}$, $\mathrm{RMSD}^2_{\rm p}$ and $\mathrm{RMSD}^2_{\rm Fe}$ depend on energy and on LIV parameter η

References

[1] R. Aloisio et al. *Phys. Rev. D* **62** (2000) 053010.
[2] L. Maccione et al. *JCAP* **04** (2009) 022.
[3] A. Saveliev, L. Maccione and G. Sigl, *JCAP* **03** (2011) 046.

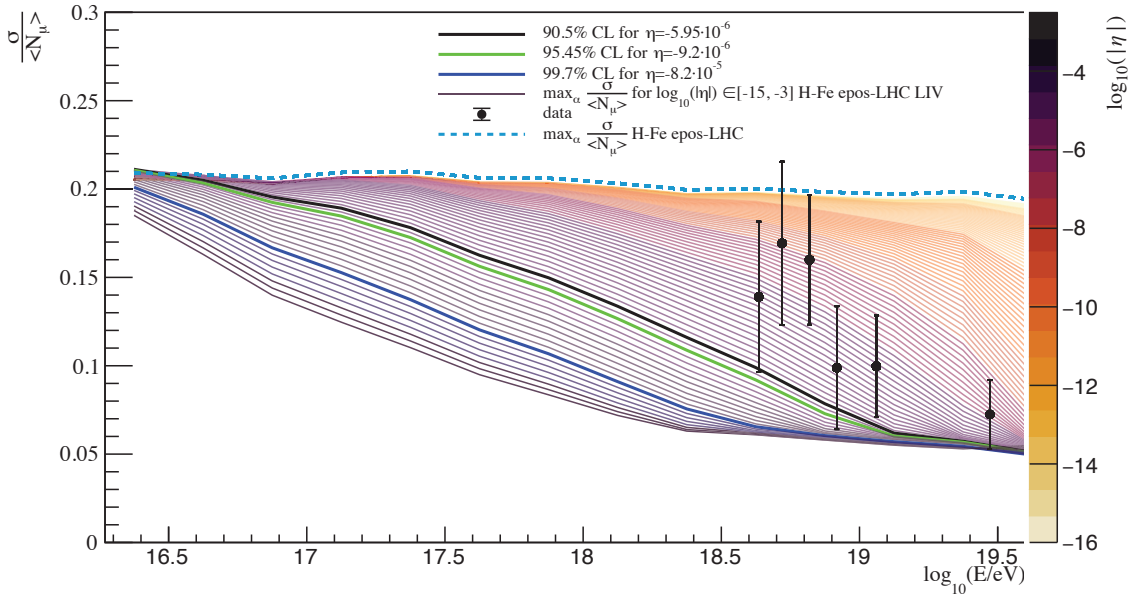

Figure 6. Maximum with respect to α of the mixed relative fluctuations obtained using the parameterizations in the standard case (dashed curve) and in the presence of LIV considering η in the range $[-10^{-3}, -10^{-15}]$ (coloured curves) as a function of the primary energy. Each color corresponds to a different violation strength (right axis). The black points with error bars (statistical uncertainties) represent the measured relative fluctuations in the number of muons. Figure from [10].

[4] L. Maccione, A. Saveliev and G. Sigl, *Proc. 12th Int. Conf. Astroparticle and Underground Physics, Munich, Germany (2011)*, PoS(TAUP2011)375.

[5] A. Aab et al. [Pierre Auger Coll.], *The Pierre Auger Observatory: Contributions to the 36th International Cosmic Ray Conference: Madison, Wisconsin, USA(2019)*, Compendium of PoS(ICRC2019).

[6] D. Boncioli et al. [for the Pierre Auger Coll.], *Proc. 34th Int. Cosmic Ray Conf., The Hague, The Netherlands (2015)*, PoS(ICRC2015)521.

[7] D. Boncioli [for the Pierre Auger Coll.], *Proc. 35th Int. Cosmic Ray Conf., Busan, Korea (2017)*, PoS(ICRC2017)561.

[8] R. G. Lang [for the Pierre Auger Coll.], *Proc. 36th Int. Cosmic Ray Conf., Madison, Wisconsin, USA (2019)*, PoS(ICRC2019)327.

[9] P. Abreu *et al.* [Pierre Auger Coll.], *JCAP* **01** (2022) no.01, 023.

[10] C. Trimarelli et al. [Pierre Auger Coll.], *Proc. 37th ICRC, Berlin, Germany (2021)*, PoS(ICRC2021)340.

[11] A. Aab et al. [Pierre Auger Coll.], *Nucl. Instrum. Meth. A* **798** (2015) 172-213.

[12] S. R. Coleman and S. L. Glashow, *Phys. Rev. D* **59** (1999) 116008.

[13] R. Alves Batista, D. Boncioli, A. di Matteo, A. van Vliet and D. Walz, JCAP **10** (2015), 063 doi:10.1088/1475-7516/2015/10/063 [arXiv:1508.01824 [astro-ph.HE]].

[14] M. De Domenico, M. Settimo, S. Riggi and E. Bertin, JCAP **07** (2013), 050 doi:10.1088/1475-7516/2013/07/050 [arXiv:1305.2331 [hep-ph]].

[15] K. Greisen, Phys. Rev. Lett. **16** (1966), 748-750 doi:10.1103/PhysRevLett.16.748

[16] G. T. Zatsepin and V. A. Kuzmin, JETP Lett. **4** (1966), 78-80

[17] A. De Angelis, G. Galanti and M. Roncadelli, Mon. Not. Roy. Astron. Soc. **432** (2013), 3245-3249 doi:10.1093/mnras/stt684 [arXiv:1302.6460 [astro-ph.HE]].

[18] R. Alves Batista, A. Dundovic, M. Erdmann, K. H. Kampert, D. Kuempel, G. Müller, G. Sigl, A. van Vliet, D. Walz and T. Winchen, JCAP **05** (2016), 038 doi:10.1088/1475-7516/2016/05/038 [arXiv:1603.07142 [astro-ph.IM]].

[19] Settimo, M. & De Domenico, M. 2013, International Cosmic Ray Conference, 33, 2488

[20] Gilmore, R. C., Somerville, R. S., Primack, J. R., et al. 2012, 422, 3189.

[21] A. J. Koning et al. TALYS 1.0. Int. Conf. on Nuclear Data for Science and Tecnology, pages 211–214, 2007.

[22] T. Pierog, I. Karpenko, J. M. Katzy, E. Yatsenko and K. Werner, *Phys. Rev. C* **92** (2015) 034906, 1306.0121].

[23] R. Aloisio, D. Boncioli, A. Di Matteo, A. F. Grillo, S. Petrera and F. Salamida, JCAP **11** (2017), 009 doi:10.1088/1475-7516/2017/11/009 [arXiv:1705.03729 [astro-ph.HE]].

[24] A. Aab *et al.* [Pierre Auger], JCAP **04** (2017), 038 [erratum: JCAP **03** (2018), E02] doi:10.1088/1475-7516/2017/04/038 [arXiv:1612.07155 [astro-ph.HE]].

[25] J. Matthews, *Astropart. Phys.* **22** (2005) 387-397.

[26] J. Linsley and A. A. Watson, *Phys. Rev. Lett.* **46** (1981) 459-463.

[27] L. Cazon, R. Conceição and F. Riehn, *Phys. Lett. B* **784** (2018) 68-76, 1803.05699].

[28] T. Pierog et al. *Nucl. Phys. B Proc. Suppl.* **151** (2006) 159-162, astro-ph/0411260].

[29] T. Bergmann et al.*Astropart. Phys.* **26** (2007) 420-432, astro-ph/0606564].

[30] S. Ostapchenko, *Phys. Rev. D* **83** (2011) 014018, 1010.1869].

[31] F. R. Klinkhamer, M. Niechciol and M. Risse, *Phys. Rev. D* **96** (2017) 116011, 1710.02507].

[32] A. Aab et al. [Pierre Auger Coll.], *Phys. Rev. Lett.* **126** (2021) 152002, 2102.07797].